Batteries
White paper

Characterization of high-voltage $Li_{1.0}Ni_{0.5}Mn_{1.5}O_4$ and correspondence between Ni content in spinel, lattice size and 4V capacity

Christian Fink Elkjær[a], Lars Fahl Lundegaard[a], Jakob Weiland Høj[a], Jonathan Højberg[a]*
Haldor Topsoe A/S, Copenhagen, Denmark
* E-mail: jhoj@topsoe.com

$Li_{1.0}Ni_{0.5}Mn_{1.5}O_4$ (LNMO) high-voltage spinel is a very promising next-generation battery cathode material.

Battery cells featuring this material have a high energy density and are significantly cheaper compared to cells with high-nickel tri-metal cathode materials such as NCA and NMC811. This is because LNMO is cobalt-free, low in nickel and has a high operating potential of 4.7 V vs. Li/Li^+. The latter also reduces the amount of anode needed to obtain a certain energy in the battery.

Introduction

The synthesis of high-quality LNMO requires a detailed understanding and stringent control of the process, because even small changes in synthesis procedure have a profound effect on material performance. In order to obtain reproducible high-quality LNMO, we have used the world-class material characterization facilities developed for the Topsoe catalyst business to map out the synthesis process. Using this knowledge, we have been able to tailor the spinel chemistry, crystal structure and surface morphology to obtain an LNMO with very low degradation and high capacity. We have labeled this material Topsoe Battery Material 129 (TBM-129).

In the development work, we analyze the materials ex situ, in situ during calcination and operando during cycling, with techniques that include X-ray diffraction, scanning electron microscopy, transmission electron microscopy, Raman spectroscopy, inductively coupled plasma optical emission spectroscopy (ICP-OES), BET surface measurement, measurement of gas evolution and a range of different electrochemical techniques. This paper provides a detailed description of the three key techniques – X-ray diffraction (XRD), transmission electron microscopy (TEM) and electrochemical screening test in half cells.

X-ray diffraction

In the technical literature, X-ray diffraction is most often used to identify the phase purity (the amount of LNMO in the material). However, careful analysis of the diffraction data makes it possible to extract much more information.

Powder X-ray diffraction data is collected on one of our analytical instruments configured in Bragg-Brentano mode using Cu Kα radiation (λ = 1.541 Å). One instrument is dedicated for high throughput ex situ analysis, which is mainly used for quality control of the LNMO products. The other instrument is dedicated for in situ calcination studies in a controlled atmosphere and for operando studies of cycling batteries (Fig. 1). For the best possible analysis, it is necessary to correct for instrument contributions to the observed data. The optics in both instruments have therefore been characterized in detail and their contribution to the observed data is included in the data analysis, which is performed using the full profile fundamental parameter approach as implemented in the TOPAS software from Bruker. As a result, very reliable and physical meaningful parameters like phase fraction, lattice parameters, crystallite size, micro strain and cation occupancies are directly obtained from the Rietveld refinement.

The spinel lattice parameter (a-axis) is, for example, determined with an uncertainty around 5/10000 Å, and the Li concentration in the tetrahedral spinel site is determined with an uncertainty of ±2%. This is the case for both ex situ quality control and for in situ calcination studies up to 1200°C. Our research has shown that even slight variations in these parameters have a significant impact on material performance and it is thus necessary to determine these with such high accuracies. Furthermore, the insight obtained with in situ XRD has enabled us to dramatically increase our understanding of the mechanisms driving the solid-state reactions at high temperature.[1]

[1] *Scientific paper in preparation.*

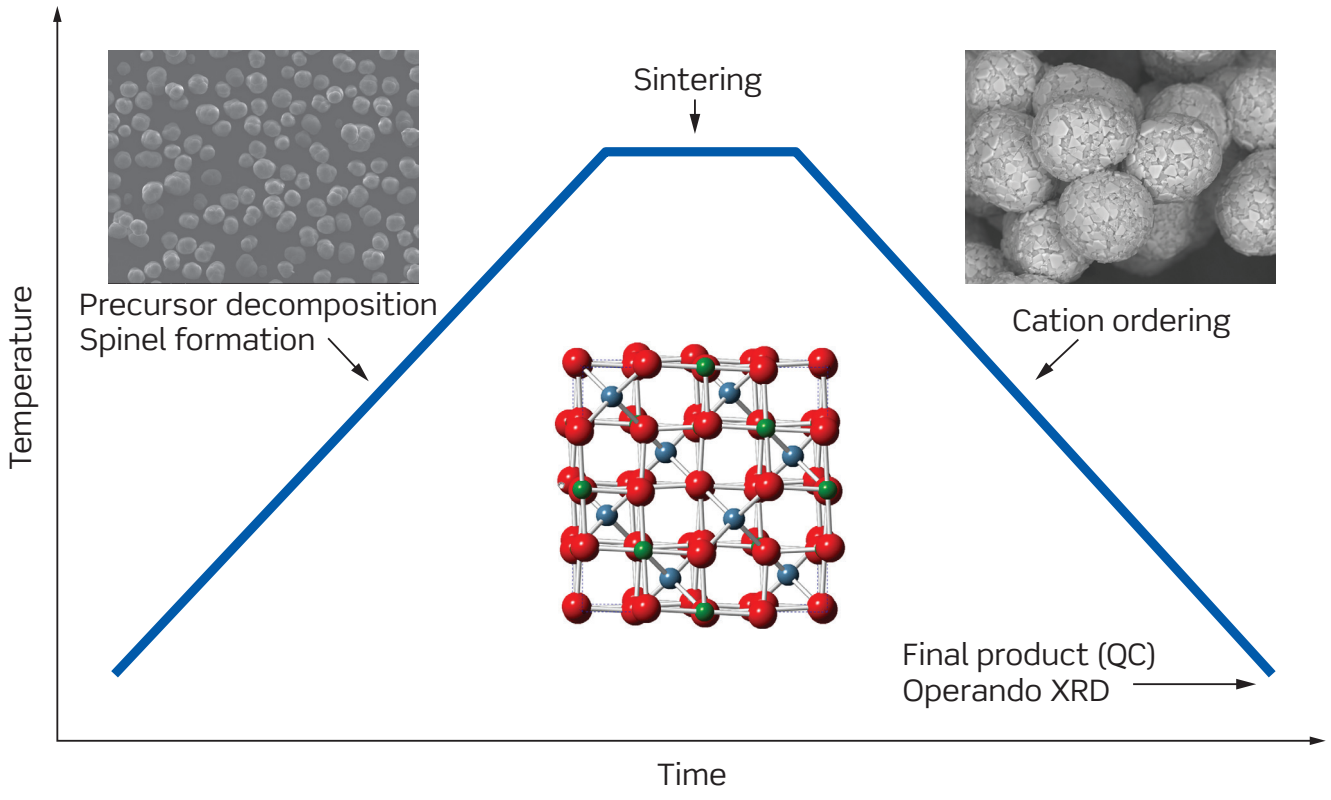

Figure 1. Schematic presentation of a temperature program used for in situ XRD studies of a number of different material processes, such as precursor decomposition, spinel formation, sintering, strain annealing and cation ordering. The SEM images in the top left and the top right show the morphology of the ~10μm precursor particles and the final spinel particles before and after the calcination process, respectively. The atomic structure of the spinel is shown in the center.

Transmission electron microscopy

TBM-129 is comprised of spherical polycrystalline particles with diameters typically in the range 5–10 µm. A scanning electron microscope (SEM) image of two such particles is shown in Fig. 2A, and reveals that the particles are highly spherical, and that the surface consists of facetted primary particles.

To investigate the internal microstructure of the material with nanometer resolution we have refined a technique to prepare very thin cross sections of the particles using a focused ion beam (FIB) and analyzed these using scanning transmission electron microscopy (STEM). Figure 2B shows an intermediate step of this preparation where material has been cut away using the FIB to reveal a freestanding cross-section of the two particles shown in Fig. 2A.

After this step, the cross-section is transferred to a suitable holder for STEM and thinned down to a thickness of 100–200 nm. Figure 2C shows the cross-section imaged in STEM using the high angle angular dark field (HAADF) technique. The material appearing with bright contrast on top of the particles is Pt, which is used in the FIB process to protect the sample. Excess material under the particles is Si from the substrate that has redistributed during cutting.

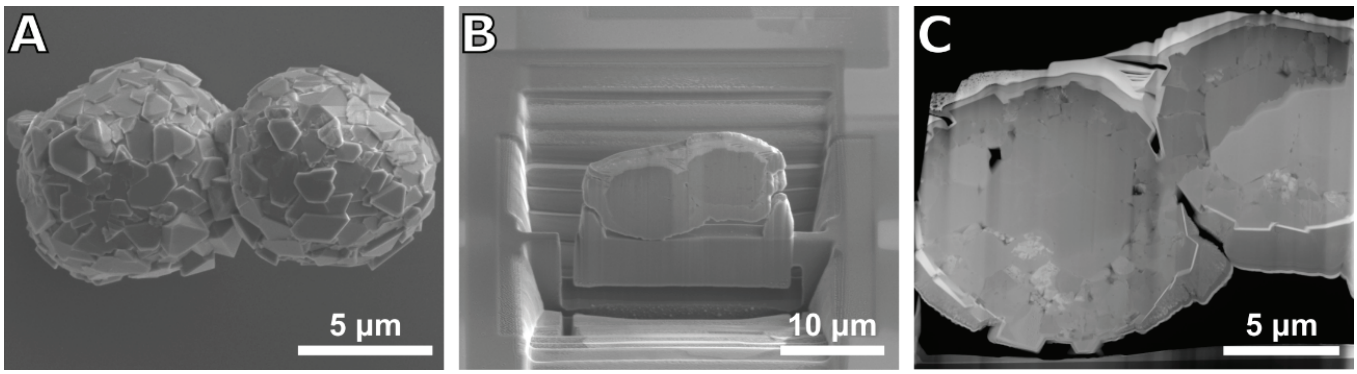

*Figure 2. Preparation of cross-sections by focused ion beam (FIB) **A**) Scanning electron microscopy (SEM) image of two TBM-129 particles on a Si substrate. **B**) A thin cross-section from the center of the particles has been cut using FIB. The layer on top of the particles with bright contrast is Pt deposited to protect the sample from the FIB during cutting. After this, the cross-section is attached to a holder for transmission electron microscopy (TEM) and thinned to a thickness of 100–200 nm. **C**) Scanning TEM (STEM) high angle annular dark field (HAADF) image of the two particles after thinning and transfer.*

Cross-sections of various LNMO materials have been imaged using STEM-HAADF and the elemental composition has been analyzed using energy dispersive x-ray spectroscopy (EDS). This technique analyzes element-specific x-rays coming from the sample during illumination by the electron beam, and produces a map showing the spatial distribution of elements in the sample. These measurements were performed on a FEI Talos transmission electron microscope equipped with the ChemiSTEM EDS detector system. The microscope was operated with an acceleration voltage of 200 kV and elemental maps were acquired and analyzed using Esprit 1.9 software from Bruker.

One challenge in the preparation of high quality LNMO is to make a material with a high phase purity. Li, Ni and Mn may form various non-LNMO phases that do not contribute to the capacity of the battery and it is therefore desirable to limit the presence of these phases to a minimum. Using STEM-EDS it is possible to image the exact position of these non-LNMO phases and measure the chemical composition of LNMO and non-LNMO phases.

Figs. 3A and 3B show a material with a phase purity of 92% (measured by XRD) and a net composition corresponding to $LiNi_{0.5}Mn_{1.5}O_4$. Figure 3A shows the HAADF image of the material where LNMO appears with grey contrast and comprises the main part of the material. The individual LNMO crystal grains comprising the particle are visible in the image, and it is evident that the crystal size varies across the particle such that the center contains very large crystals in the order of 1–2 µm and the part closer to the surface is comprised of smaller crystals. The elemental map (Fig. 3B) reveals that the LNMO phase is very homogeneous with the same amount of Mn and Ni across the particle. The non-LNMO phases appear with bright green contrast and contain a much higher amount of Ni compared to the LNMO. A detailed quantification of the material composition is presented later in Fig. 4.

Figs. 3C and 3D show a material with a very high phase purity of 99% (measured by XRD) and a net composition corresponding to $LiNi_{0.4}Mn_{1.6}O_4$. Contrary to the previous example, this material is comprised of small crystallites typically in the range 0.2–0.5 µm across the particle. Only LNMO spinel phase can be identified in the image and elemental map, supporting the fact that this is a material with a high phase purity.

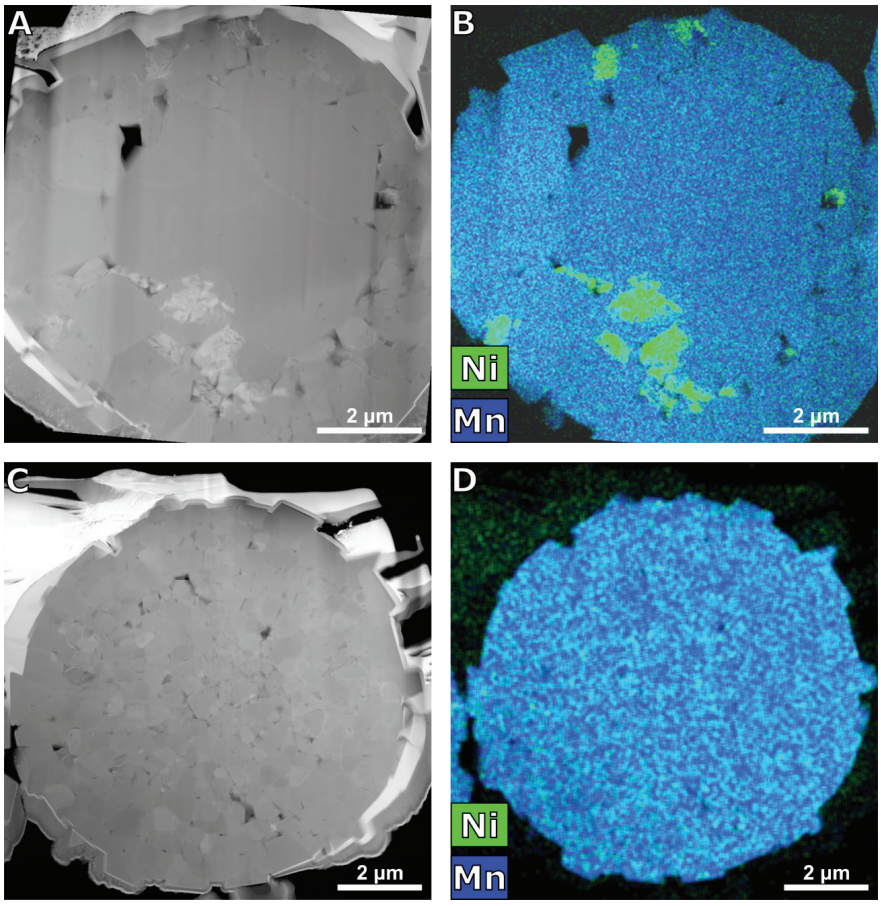

*Figure 3. Internal structure and phase purity. **A**) STEM HAADF image and **B**) elemental map of an LNMO material characterized by large primary crystallites in the center and incomplete phase purity (92% LNMO as measured by XRD). Non-LNMO phases are seen as Ni-rich regions in the elemental map. **C**) STEM HAADF image and **D**) elemental map of an LNMO material characterized by smaller primary crystallites and very high phase purity (99% LNMO as measured by XRD), which is also confirmed by the elemental map.*

A closer look at the lower left area of the particle shown in Figs. 3A and 3B enables a detailed quantification of the chemical composition of the LNMO and non-LNMO phases for this material. The quantification provides atomic percentages of the elements present in the sample, which in this case are Ni, Mn and O.

The EDS technique is not able to measure the presence of Li. In order to easily relate the composition to the chemical formula of LNMO, all elements were normalized to the sum of Ni and Mn such that Ni+Mn=2.

Two areas are selected for quantification in Fig. 4B; the blue area is LNMO and the green area is the Ni-rich non-LNMO phase. The composition of the LNMO phase is measured to $Ni_{0.45}Mn_{1.55}$ and for the non-LNMO phase it is $Ni_{1.26}Mn_{0.74}$, i.e. very high in Ni compared to the LNMO.

This sample is made from a precursor with a net chemical composition of $Ni_{0.5}Mn_{1.5}$ but prepared in such a way that the actual LNMO composition has a lower Ni content and we see that the excess Ni is located in the Ni-rich non-LNMO phase.

In order to prepare materials with high phase purity, it is thus crucial to synthesize the sample in a way that favors an LNMO composition as close as possible to the composition of the precursor.

Through our research, we have learned to control the composition of the LNMO and TBM-129 is thus a material with a high phase purity and high resulting capacity.

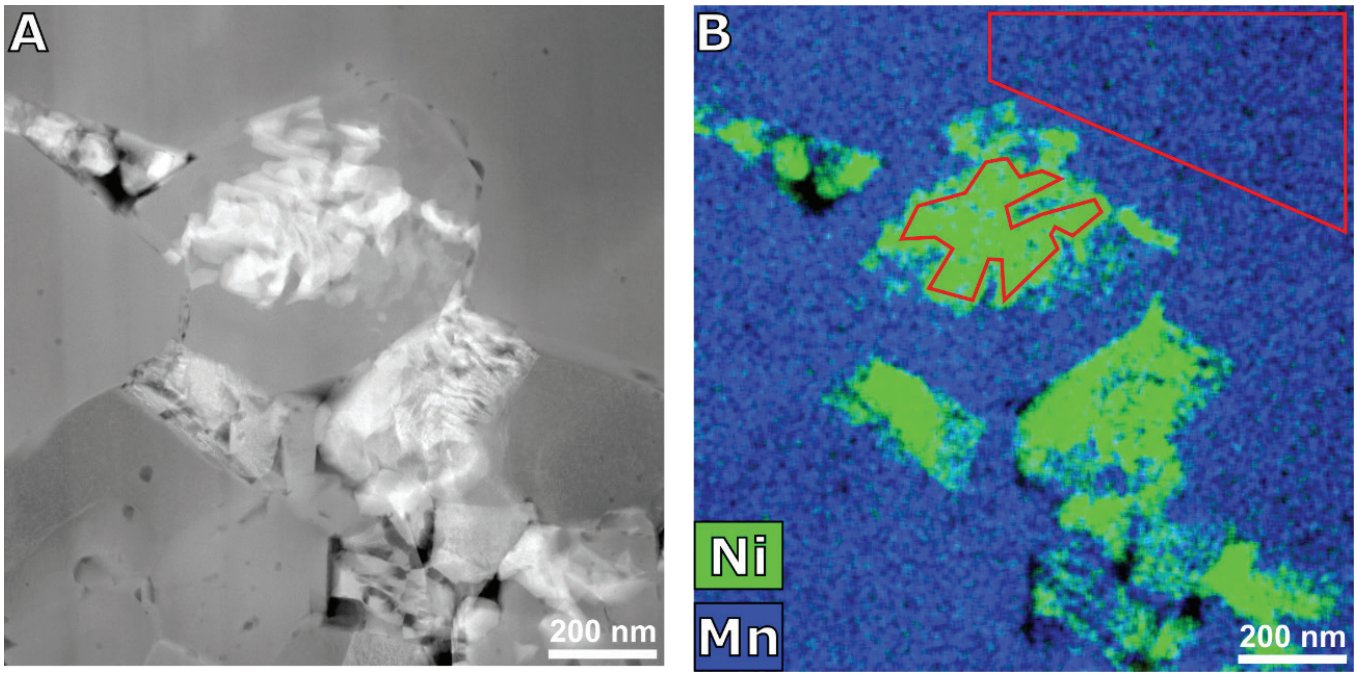

*Figure 4. Composition of LNMO and non-LNMO phase. **A**) STEM HAADF image and **B**) elemental map of LNMO and non-LNMO phases in close proximity. Quantification of the elemental map reveals that the composition of the LNMO phase corresponds to $Ni_{0.45}Mn_{1.55}$ (blue area marked by red line) and the composition of the non-LNMO phase corresponds to $Ni_{1.26}Mn_{0.74}$ (green area marked by red line). The EDS technique is not able to measure the amount of Li.*

Electrochemical screening in half cells

Literature describing electrochemical tests of battery materials provides many electrochemical test procedures and the choice of method depends on the scope of the test. Our internal screening of materials has three main criteria: 1. The procedure should be fast in order to speed up the development process, 2. The procedure should be robust in order to reliably compare different LNMO materials where e.g. synthesis route, chemical composition or particle characteristics vary, 3. The procedure should retrieve important material characteristics such as specific capacity, power capability, capacity fade and 4V capacity. The latter is discussed further below.

To screen fast, we do lab scale half cell tests in 2032 type coin cells. We test at 55°C in order to speed up degradation reactions and include a power test with 10C discharge to stress the material. To ensure a robust screening, we use low electrode loading of 0.7 mAh/cm^2 and high amount of carbon and binder (8wt% each) to ensure that we test the properties of the material rather that our ability to make the individual electrodes. We use commercially available battery components and materials such as Super C65 carbon black (Timcal), PVdF binder (polyvinylidene difluoride, Sigma Aldrich) and NMP (N-methyl-pyrrolidone, VWR) for the slurry, coin cell parts from MTI Corp. and Hohsen Corp., 250 µm precut lithium disc (MTI Corp.), polymer separator (Toray V25EKD and Freudenberg FS2192-11SG) and 1 M $LiPF_6$ in EC:DMC (1:1 w/w) (E001, Solvionic).

Slurries are spread onto carbon coated aluminum foil (MTI) using a doctor blade with a 100–200 µm gap and dried for 12 hours at 80°C. Electrodes are cut from the dried films with a diameter of 14 mm, pressed in a hydraulic pellet press with 3 tons followed by 10 hours drying at 120°C under vacuum in an argon-filled glove box.

To retrieve the relevant material characteristics, the electrochemical test contains 6 formation cycles (3 cycles 0.2C/0.2C (charge/discharge) and 3 cycles 0.5C/0.2C), 25 power test cycles (5 cycles 0.5C/0.5C, 5 cycles 0.5C/1C, 5 cycles 0.5C/2C, 5 cycles 0.5C/5C, 5 cycles 0.5C/10C) followed by 120 0.5C/1C cycles to measure degradation. C-rates are calculated based on the theoretical specific capacity of the cathode material of 147 mAhg^{-1}; thus, for example 0.2C corresponds to 29.4 mAg^{-1} and 10C corresponds to 1.47 Ag^{-1}. The 4V capacity is calculated based on cycle 3, the specific capacity is calculated based on cycle 7 (0.5C/0.5C), the power capability is the ratio between capacity at cycle 7 and cycle 29 (0.5C/10C), and the degradation is calculated between cycle 33 and cycle 133.

The 4V capacity quantifies the capacity between 3.5 V and 4.3 V vs. Li/Li$^+$ compared to the total capacity between 3.5 V and 5.0 V vs. Li/Li$^+$. It is an important quantity because it relates to the amount of Mn^{3+} in the LNMO structure as will be further described in the next section. The 4V capacity is calculated as an average between discharge and charge, because the cell is not in equilibrium during cycling.

This shifts voltages upwards during charge and downwards during discharge due to internal resistance in the cell. This effect is especially pronounced near sudden changes in cell voltage and the fraction of Mn activity will therefore appear different depending on whether the analysis is based on a charge or a discharge. Using parameters defined in Fig. 5, the 4V capacity is calculated based on the third cycle at 0.2C as (Q^{4V}_{cha} + (Q^{tot}_{dis} -Q^{4V}_{dis})) / (2*Q^{tot}_{dis}).

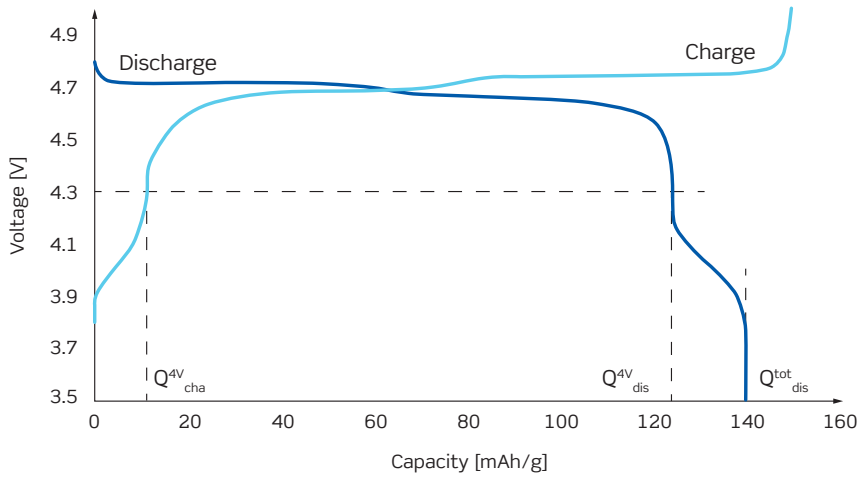

Figure 5. Discharge and charge voltage curves of LNMO half cell. The capacities Q^{4V}_{cha}, Q^{4V}_{dis} and Q^{tot}_{dis} are used to calculate the 4V capacity.

Correspondence between Ni content in spinel, lattice size and 4V capacity

By combining high-quality characterization with electrochemical testing and detailed data analysis, we have been able to demonstrate a close correspondence between the Ni content in the spinel, the lattice size and the 4V capacity. To our knowledge, this correspondence has not been reported elsewhere.

The Ni content in the spinel is determined using STEM-EDS by specifically identifying the spinel phases and quantifying the composition of these. The lattice size of the spinel is determined using XRD and the 4V capacity is determined electrochemically. Figs. 6A and 6B show the close correspondence between the Ni content in the spinel, the lattice size and the 4V capacity.

The reason for the correspondence is that variations in the Mn/Ni ratio change the ratio between Mn^{3+} and Mn^{4+}. This is apparent by calculating the average oxidation state of Mn in $LiNi_yMn_{2-y}O_4$ as (4*2-1-2*y)/(2-y) based on the assumption that the oxidation state of Li is 1+, Ni is 2+ and O is -2. Using this, the formula can be written as $Li^{+1}Ni^{+2}_yMn^{+3}_{1-2y}Mn^{+4}_{1+y}O_4$.

In X-ray diffraction, a change in the Mn/Ni ratio will change the lattice parameter because the sizes of Mn^{3+} and Mn^{4+} ions in the spinel are different. The exact correspondence between the a-axis and the Mn/Ni ratio must be determined empirically.

Electrochemically, Mn^{3+}/Mn^{4+} reactions are observed around 4 V vs. Li/Li^+ and Ni^{2+}/Ni^{4+} reactions are observed around 4.7 V vs. Li/Li^+, and therefore a change in Mn/Ni ratio will change the 4V capacity. In LNMO, Mn^{3+} can be oxidized reversibly to Mn^{4+} and back by extraction and insertion of Li+ during cycling, and Ni^{2+} can be oxidized reversibly to Ni^{4+} and back by extraction and insertion of Li^+ during cycling. It is thus possible to extract (and subsequently insert) two Li^+ per Ni^{2+} and one Li^+ per Mn^{3+}. Based on the formula $Li^{+1}Ni^{+2}_yMn^{+3}_{1-2y}Mn^{+4}_{1+y}O_4$, the share of capacity related to Mn activity compared to the total capacity is thus given by (1-2y)/(1-2y + 2y) = (1-2y). It is therefore possible to directly calculate the Ni content based on the 4V capacity and vice versa. As an example, y=0.5 corresponds to 0% 4V capacity and y=0.45 and 0.4 correspond to 10% and 20% 4V capacity, respectively.

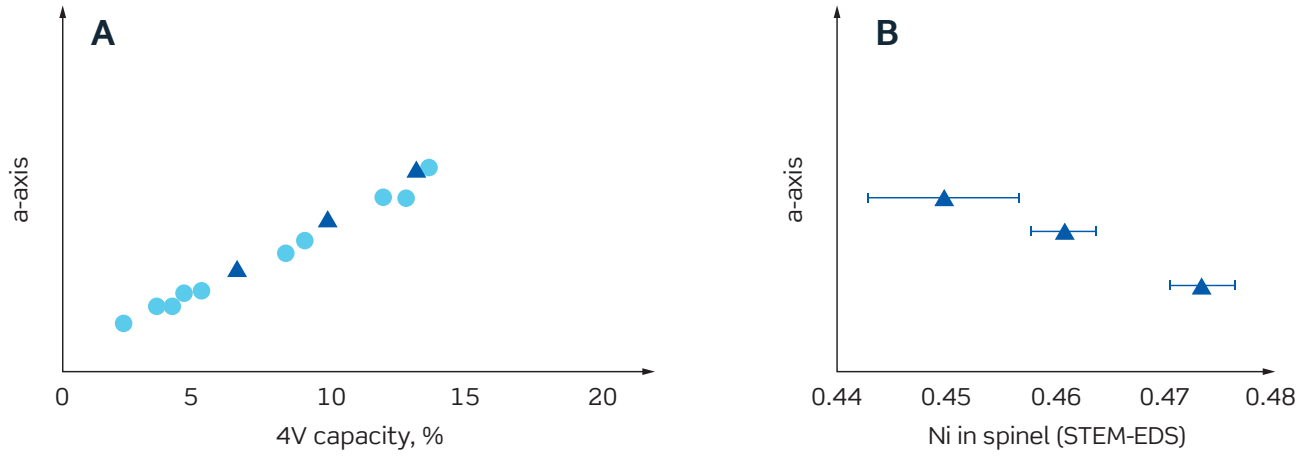

*Figure 6. Correspondence between **A**) 4V capacity and lattice size (a-axis) and **B**) Ni content in the spinel and lattice size (a-axis). The data in **B** is represented by triangles in **A**.*

Using these correspondences, it is possible to calculate the Ni content in the LNMO spinel based on 4V capacity and XRD, and compare this to the values measured using STEM-EDS. These values are compared in Table 1 and Figure 7 for the three samples shown in Figure 6B. It is noted that the lack of correspondence between Ni in the net chemical composition and in the LNMO spinel stresses the importance of understanding this correspondence when developing LNMO.

TABLE 1
Correspondence between Ni content in the LNMO spinel determined based on STEM-EDS, 4V capacity and XRD. The data is plotted in Figure 7.

Net chemical composition	STEM-EDS	4V capacity	XRD
0.46	0.461	0.458	0.458
0.5	0.450	0.444	0.446
0.46	0.474	0.473	0.477

Ni content y in the spinel $LiNi_yMn_{2-y}O_4$

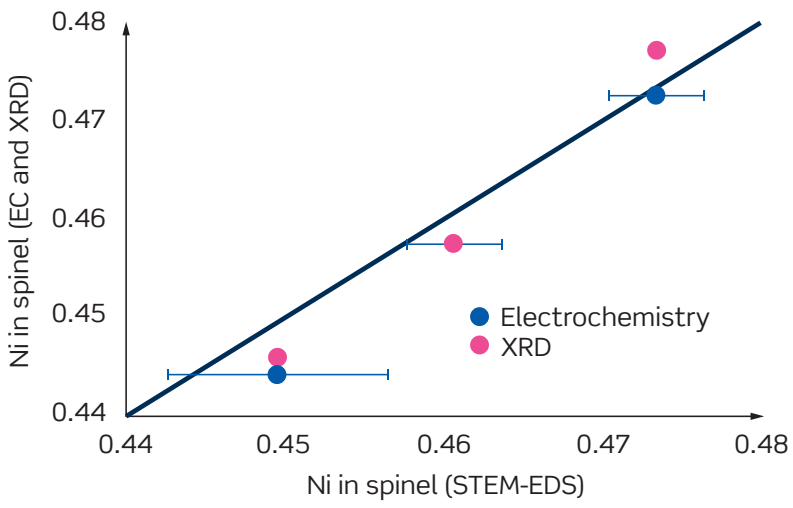

Figure 7. Correspondence between Ni content in the LNMO spinel determined based on STEM-EDS and Ni content in the LNMO spinel determined based on electrochemistry (4V capacity) and XRD (a-axis). Data is listed in Table 1.

About TBM-129

Topsoe Battery Material 129 (TBM-129) is an LNMO high-voltage spinel material. TBM-129 is developed to have good powder properties, high tap density and low degradation. This is obtained by precipitating spherical precursor particles and by a proprietary calcination process.

The process makes it possible to adjust the particle size distribution and obtain tap densities above 2.3 g/cm^3. The degradation rate and rate of Mn-Ni dissolution at 55°C are very low and can be reduced still further by doping and coating.

Figure 8.
***A**) SEM picture of a typical TBM-129 LNMO particle.*

***B**) Half cell benchmark test at 55°C of TBM-129 and TBM-129e (engineered TBM-129) with three commercially available references. The test shows that TBM-129 has higher capacity and lower degradation than reference samples, and that engineering of TBM-129 can further decrease degradation significantly.*

***C**) Full cell data of untreated LNMO with graphite (light blue) and LTO (dark blue) anodes tested at 25°C using standard 1 M $LiPF_6$ in EC:DMC electrolyte.*

A

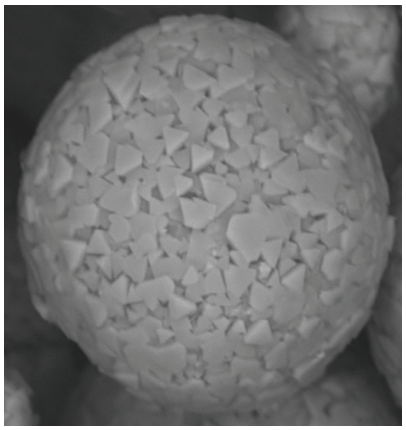

B

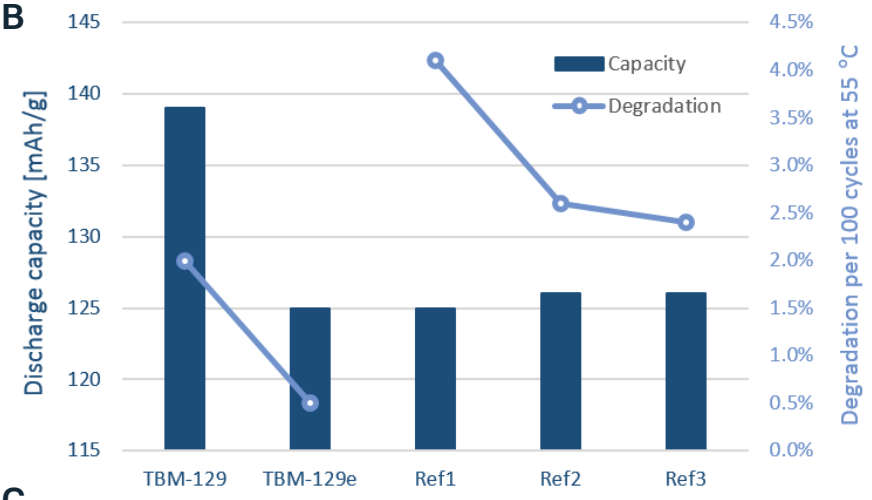

C

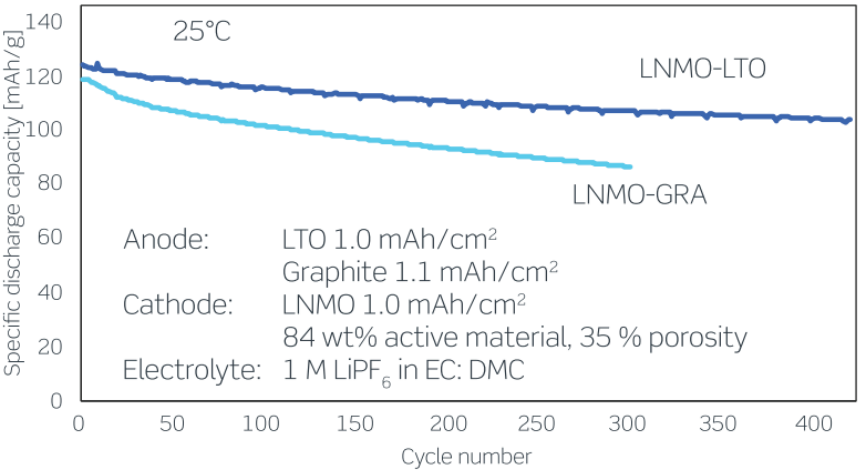

About Haldor Topsoe A/S

Haldor Topsoe is a world-leader in catalysis and surface science, committed to helping our customers achieve optimal performance. We enable companies to get the most out of their processes and products, using the least possible energy and resources, in the most responsible way.

The development of better battery materials for rechargeable batteries is key to the future of many industries. Utilizing our long history within catalysis and surface science; from product development at the nanoscale to fully industrialized manufacturing at ton-scale we are developing the next generation battery materials for rechargeable batteries that will be safer, lighter, more durable, faster to charge, more powerful and cost-efficient.

We are headquartered in Denmark and do project development, R&D, engineering, production, and sales & service across the globe.

Get in touch today:
www.topsoe.com/batteries

Haldor Topsoe A/S, cvr 41853816 | GMC | 0283.2019/Rev.0